

# Human-like Dexterous Manipulation for the Anthropomorphic Hand-arm Robotic System via Teleoperation

Yayu Huang<sup>1,2</sup>, Zhenghan Wang<sup>1,2</sup>, Xiaofei Shen<sup>1</sup>, Qian Liu<sup>1</sup>, and Peng Wang<sup>1,2,3</sup> (✉)

<sup>1</sup> Institute of Automation, Chinese Academy of Sciences, Beijing 100190, China  
peng.wang@ia.ac.cn

<sup>2</sup> School of Artificial Intelligence, University of Chinese Academy of Sciences, Beijing 100049, China

<sup>3</sup> Centre for Artificial Intelligence and Robotics, Hong Kong Institute of Science and Innovation, Chinese Academy of Sciences, Hong Kong 999077, China

**Abstract.** Teleoperation has the potential to enable robots to replace humans in high-risk scenarios and catastrophic events, performing manipulation tasks efficiently and securely under human guidance. However, achieving human-like dexterous manipulation remains challenging, particularly for anthropomorphic hand-arm robotic systems with high degrees of freedom. Accurately capturing the operator’s motion and providing real-time intuitive feedback to enhance the sense of telepresence place substantial demands on human-robot perception and interaction. Moreover, the inherent physical and functional differences between anthropomorphic hand-arm robots and humans pose challenges in ensuring the accuracy and reliability of dexterous teleoperation. To overcome these challenges, we present an integrated approach involving an anthropomorphic hand-arm robot system, a wearable motion capture and force feedback system, and a set of motion mapping and force mapping methods. We conducted experiments on both simulation and real-world platforms to evaluate the usability and effectiveness of our proposed approach, with the results demonstrating significant advancements in achieving human-like dexterity via teleoperation.

**Keywords:** Dexterous Manipulation · Teleoperation · Anthropomorphic hand-arm robots · Motion mapping · Force mapping.

## 1 Introduction

Advances in robotics manufacturing and artificial intelligence technologies have enabled researchers to achieve autonomous dexterous manipulation in anthropomorphic robots[1,2,3,4,5,6]. While offering great potential for solving complex and dexterous manipulation tasks, the unreliability and instability of autonomous learning pose challenges for its application in sophisticated scenarios. To address this, human-like dexterous manipulation via teleoperation has

emerged as a viable solution, serving as a bridge between humans and robots. By combining the decision-making experience of human intelligence with the powerful manipulation capabilities of robots, teleoperation allows robots to effectively replace humans and perform intricate manipulations in environments that are either inaccessible or hazardous to human operators. This approach has found widespread use in various real-world domains, including industrial production, medical treatment, mining, and explosive ordnance disposal. Nevertheless, achieving human-like dexterous teleoperation in anthropomorphic robots presents a complex and multifaceted challenge. Precisely capturing human motion and providing real-time force feedback prove to be demanding tasks. Moreover, the disparities between anthropomorphic robots and humans in physical aspects such as size, weight, and kinematics, as well as functional aspects such as sensing, actuation, force, and velocity, further complicate the realization of seamless teleoperation. Consequently, a comprehensive dexterous teleoperation system necessitates the careful consideration of three fundamental sub-problems: how to capture human motion, how to map human motion to the robot effectively, and how to give feedback to the human on the forces perceived by the robot.

In this paper, we present a comprehensive framework that addresses the challenges of achieving human-like dexterous manipulation in anthropomorphic hand-arm robot systems through teleoperation, focusing on the three subproblems mentioned earlier. Firstly, we develop a wearable system utilizing a data glove and three IMUs (Inertial Measurement Units) to accurately capture human hand-arm motion. Next, we propose two distinct mapping methods: a hybrid mapping approach for hand motion mapping and a motion modification approach for arm motion mapping. These methods are effective in accurately translating human motions to the robot. Finally, we introduce a force-feedback system based on a hand exoskeleton, which utilizes a nonlinear mapping method to enhance the operator’s sense of immersion by mapping the perceived force from the robot to the operator.

The subsequent sections of this paper are organized as follows. Sect. 2 provides a comprehensive overview of related work on motion capture of human hands, human motion mapping, and feedback in teleoperation. In Sect. 3, we present the proposed framework for achieving human-like dexterous manipulation via teleoperation. The specific methods utilized, including the hand motion mapping method, the arm motion mapping method, and the force mapping law, are detailed in Sect. 4. To validate the effectiveness of the framework, experimental results obtained from both simulation and real-world platforms are presented in Sect. 5. Finally, we give a conclusion in Sect. 6.

## 2 Related Work

### 2.1 Motion Capture of Human Hands

Capturing human motion, especially human hand motion can be achieved in a visual way or a haptic way[7].

Vision-based methods typically rely on camera input to capture motion. Some works extract motion information, such as wrist pose, hand pose parameters, hand shape parameters, and keypoint positions, from the visual data[8,9].[8,9]. Still, other works do not focus on specific motion information but directly predict the pose of the robot hand that is visually similar to the human hand pose[10]. Vision-based approaches offer advantages in terms of cost-effectiveness and ease of deployment but are limited by camera capabilities and algorithms. Furthermore, the absence of haptic feedback represents a significant drawback.

Haptic-based approaches, on the other hand, rely heavily on wearable devices to estimate human posture and obtain feedback. Data gloves are the most common type of wearable device, providing information such as the position and motion of the fingers and the whole hand, as well as haptic feedback information. Exoskeletons are typically worn on the dorsum and involve rigid links for providing kinesthetic feedback to the hand. Haptic-based approaches, although more complex and costly to implement, offer the significant advantage of providing controllable motion and feedback.

In this work, we target to design a haptic-based system that captures human hand-arm motion, making teleoperation controllable and realistic.

## 2.2 Human motion mapping

Mapping human motion onto a hand-arm robot is another key problem in teleoperation, where the difficulty comes from the mismatch between human and robot including workspace, configuration, and manipulation resolution[11]. The problem is commonly decomposed into two parts to be considered: hand-motion mapping and arm-motion mapping.

The most frequently used methods for hand motion mapping are direct Cartesian mapping and direct joint mapping. Direct Cartesian mapping involves scaling, optimizing, or transforming the fingertip positions of the human hand and leading the robot fingertip to that specified position. This method is applicable to various robotic hands but is limited to precision grasps. Direct joint mapping directly employs the corresponding joint values of the human hand to control the robot hand. This method is intuitive and straightforward but only suitable for robots with similar kinematics to the human hand. In this work, we aim to design a hybrid mapping algorithm that combines the advantages of both methods. This hybrid mapping algorithm is intended to be simpler, more intuitive, easier to implement, and collision-free compared to previous algorithms[12,13].

In the context of arm motion mapping, two categories can be distinguished: direct mapping and motion modification[14]. The former directly utilizes the original human demonstration data (joint angles, positions, trajectories) without modification, which is simple and intuitive but does not consider the differences in body structure and size. The latter addresses the variations in body structure and size by scaling the obtained human position data, resulting in a more reasonable mapping. Therefore, in this work, we employ the motion modification method to the changes in the human hand position, thus achieving more natural teleoperation of the robotic arm.

### 2.3 Feedback in teleoperation

Feedback is crucial in teleoperation, and while visual feedback is essential for providing information about the position and objects in the remote environment, haptic feedback becomes paramount as the robot approaches objects and vision becomes occluded. Realistic, accurate, and low-delay haptic feedback serves as a vital source of human-robot interaction information, greatly enhancing the operator's sense of immersion. Haptic feedback can be categorized into tactile feedback, which enables the perception of object texture and shape, and kinesthetic feedback, which allows for the perception of force and contact. In this work, we investigate the force-feedback system, where the hand exoskeleton serves as an interface between the human and the robot.

## 3 Framework

Our objective is to develop a framework for human-like dexterous manipulation via teleoperation for the anthropomorphic hand-arm robotic system. This framework empowers operators to perform natural motions, guiding the robot to execute various intricate manipulations. An overview of the framework is depicted in Fig.1.

The **interaction system** serves as the interface between the operator and the robot, capturing human motions and providing feedback. Human finger motions and arm motions are measured by a data glove and three IMUs attached to the upper arm, forearm, and hand, respectively. The estimated angle information is converted into position information through forward kinematics. The hand motion mapping method and the arm motion mapping method are then employed to determine the hand and arm joint angles of the robot, respectively.

The **hand-arm robotic system** consists of a robotic arm and a CASIA Hand, which features 25 joint degrees of freedom and 21 degrees of actuation, with a force sensor attached to each fingertip. The desired joint angles are executed by the robot controller. During interactions with the environment, force information is generated and processed according to a specific force mapping law. This force feedback is naturally conveyed to the operator through the wearable hand exoskeleton, enhancing their perception of the robot's contact forces.

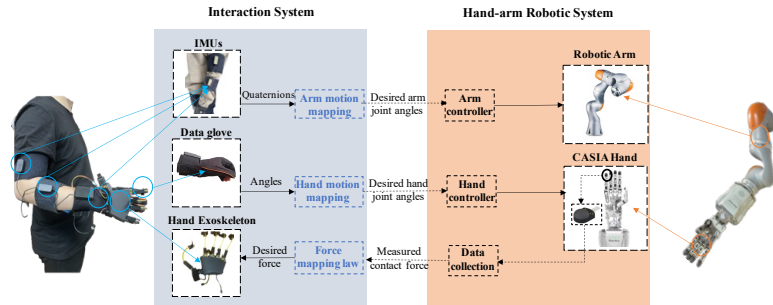


**Fig. 1.** The framework of human-like dexterous manipulation for the anthropomorphic hand-arm robotic system via teleoperation.

## 4 Methods

### 4.1 Hand Motion Mapping

Our objective is to develop a hybrid mapping method that leverages the advantages of both direct Cartesian mapping and direct joint mapping approaches. For this purpose, we utilize MANO [15], which represents the human hand with 15 ball joints and 15\*3 degrees of freedom. To align it with the structure of the actual human hand, we simplify the model to have 20 degrees of freedom, with 4 degrees of freedom assigned to each finger. Fig.2(a) shows the differences in kinematic structure between the simplified MANO model and the CASIA Hand.

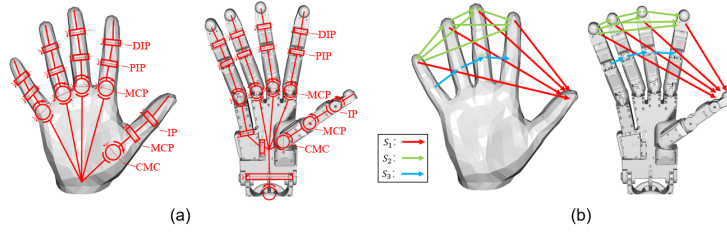


**Fig. 2.** MANO and CASIA Hand. (a) Kinematic structure. (b) Vector group.

Considering the factors of fingertip orientation and distance, joint angle, and self-collision, we follow DexPilot[16] to formulate the hand motion mapping problem as a non-linear optimization problem, with the specific objective function:

$$\min \sum_{i=1}^n w_1(d_i) \|v_i(q_t^{RH}) - s(d_i)\hat{v}_i(q_t^{MH})\|^2 + w_2(d_i) \|q_t^{RH} - q_t^{MH}\| + w_3 \|q_t^{RH} - q_{t-1}^{RH}\|^2 \quad (1)$$

Where  $q_t^{MH}$ ,  $q_t^{RH}$  respectively represent the joint angles of MANO and CAISA Hand at time  $t$ ,  $v_i(q_t^{MH}) \in \mathbb{R}^3$ ,  $v_i(q_t^{RH}) \in \mathbb{R}^3$  respectively represent the vectors obtained by forward kinematics of MANO and CAISA Hand in the world coordinate system, pointing from one key point to another, as shown in Fig.2(b).  $n$  represents the total number of vectors. Furthermore,  $d_i = \|v_i(q_t^{MH})\|$  and  $\hat{v}_i(q_t^{MH}) = \frac{v_i(q_t^{MH})}{\|v_i(q_t^{MH})\|}$ .  $q_t^{RH}$  and  $q_t^{MH}$  are the structurally corresponding joints in the MANO and CASIA Hand, including the DIP, PIP, and MCP joints of the index, middle, ring, and little fingers.

The distance coefficient function  $s(d_i)$  is defined as:

$$s(d_i) = \begin{cases} \eta_1, & d_i \leq \varepsilon \wedge v_i(q_t^{RH}) \in S_1 \\ \eta_2, & d_i \leq \varepsilon \wedge v_i(q_t^{RH}) \in S_2 \\ \eta_3, & d_i \leq \varepsilon \wedge v_i(q_t^{RH}) \in S_3 \\ \alpha d_i, & d_i > \varepsilon \end{cases} \quad (2)$$

Where  $\varepsilon$  is the distance threshold parameter, the scaling factor  $\alpha = 1.5$  represents the difference in size between CASIA hands and MANO,  $\eta_1 = 1 \times 10^{-4}$ m keeps the thumb fingertip close to the other fingertip during precision grasp,  $\eta_2 = 0.025$ m and  $\eta_3 = 0.03$ m force a safe distance between fingertips and between the neighboring joints to avoid collisions. The weight coefficient function  $w_1(d_i)$  is defined as:

$$w_1(d_i) = \begin{cases} \mu_1, & d_i \leq \varepsilon \wedge v_i(q_t^{RH}) \in S_1 \\ \mu_2, & d_i \leq \varepsilon \wedge v_i(q_t^{RH}) \in S_2 \\ \mu_3, & d_i \leq \varepsilon \wedge v_i(q_t^{RH}) \in S_3 \\ \mu_4, & d_i > \varepsilon \end{cases} \quad (3)$$

Where  $\mu_1 = 45$ ,  $\mu_2 = 50$ ,  $\mu_3 = 25$  and  $\mu_4 = 10$ . The weight coefficient function  $w_2(d_i)$  is defined as:

$$w_2(d_i) = \begin{cases} \lambda_1, & d_i > \varepsilon_2 \wedge v_i(q_t^{RH}) \in S_1 \\ \lambda_2, & d_i \leq \varepsilon_2 \wedge d_i > \varepsilon_1 \wedge v_i(q_t^{RH}) \in S_1 \\ \lambda_3, & d_i \leq \varepsilon_1 \wedge v_i(q_t^{RH}) \in S_1 \end{cases} \quad (4)$$

Where  $\lambda_1 = 0.1$ ,  $\lambda_2 = 0.05$ ,  $\lambda_3 = 0.01$ ,  $\varepsilon_1 = 0.02$  and  $\varepsilon_2 = 0.04$ . These values are chosen to ensure reasonableness, considering that precision grasp is more likely than power grasp when the thumb is too close to the other fingers, and thus the attention to joint similarity should be reduced. Additionally, we added an L2 normalization term with  $w_3 = 1 \times 10^{-3}$  to improve smoothness and temporal consistency.

For implementation, we use Sequential Least-Squares Quadratic Programming (SLSQP) algorithm in NLopt[17] to optimize the above objectives in real-time.

## 4.2 Arm Motion Mapping

The arm motion mapping algorithm aims to enable the dexterous robot hand to replicate the motion of the operator's hand in Cartesian space, ensuring controllability during operation. To simplify the process, we focus only on the hand's position and orientation, disregarding the arm shape that aims to maintain similarity between the human and the robot. Consequently, it becomes essential to calculate the relative position and orientation of the human hand based on the data obtained from the three IMUs. We model the human arm as a 7-degree-

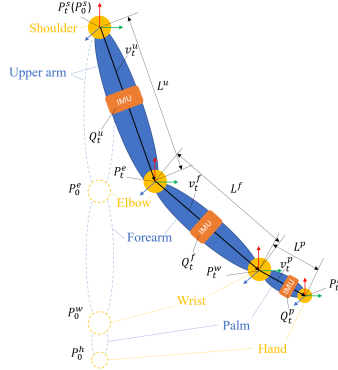


**Fig. 3.** Diagram of the human arm model.

of-freedom system, with 3 degrees of freedom for the shoulder joint, 1 degree of freedom for the elbow joint, and 3 degrees of freedom for the wrist joint.

Three IMUs are attached to the upper arm, forearm, and hand, respectively, and they are calibrated to the initial state where the arm naturally hangs down and the palm faces toward the body. As shown in Fig.3, the following variables are defined:

- The length of each link: upper arm  $L^u$ , forearm  $L^f$ , hand  $L^p$ .
- The quaternion of each link at time  $t$ : upper arm  $Q_t^u$ , forearm  $Q_t^f$ , palm  $Q_t^p$ .
- The position of each joint at time  $t$ : shoulder joint  $P_t^s$ , elbow joint  $P_t^e$ , wrist joint  $P_t^w$ .
- The vector of each link at time  $t$ : upper arm  $v_t^u$ , forearm  $v_t^f$ , hand  $v_t^p$ .

The position of the hand  $P_t^h$  at time  $t$  is:

$$P_t^h = P_0^s + Q_t^u * v_0^u + Q_t^f * v_0^f + Q_t^p * v_0^p \quad (5)$$

Where the operation rule for multiplying a quaternion by a vector is defined as:

$$Q * v = Im(Q \otimes v \otimes Q^{-1}) \quad (6)$$

In order to cope with the difference in structure and size between the human arm and the robotic arm, the changes in the position of the human hand are modified to yield the target position of the robotic hand.

$$pos_t^{TA} = [\rho_1 \ \rho_2 \ \rho_3] \cdot (P_t^h - P_0^h) + pos_0^{RA} \quad (7)$$

where  $pos_t^{TA}$  is the target position of the robotic hand at time  $t$ ,  $\rho_1, \rho_2, \rho_3$  are scaling factors, and  $pos_0^{RA}$  is the initial position of the robot hand.

It is worth noting that the slave arm includes all degrees of freedom of the robotic arm and two degrees of freedom of the CASIA wrist. We formulate the arm motion mapping as an optimization problem, the optimization objective is:

$$\min w_{pos} \|pos(q_t^{RA}) - pos_t^{TA}\|^2 + w_{quat} (1 - \langle quat(q_t^{RA}), quat_t^{TA} \rangle)^2 + \beta \|q_t^{RA} - q_{t-1}^{RA}\|^2 \quad (8)$$

Where  $q_t^{RA}$  represents the joint angles of the robotic arm at time  $t$ , while  $pos(q_t^{RA})$  and  $quat(q_t^{RA})$  respectively indicate the position and rotation of the CASIA Hand at time  $t$ . It is worth noting that  $quat_t^{TA}$  is equivalent to the previously mentioned  $Q_t^p$ .  $\langle q_1, q_2 \rangle$  denotes the inner product of the corresponding quaternions. As with the hand motion mapping, the objective function includes an L2 normalization term to improve smoothness and temporal consistency and likewise optimizes the above objective in real-time using Sequential Least-Squares Quadratic Programming (SLSQP) algorithms in NLOpt[17].

### 4.3 Force Mapping Law

Force mapping involves transferring the force experienced by the robot's fingertips to the operator's hands. The level of realism in force transfer directly influences the operator's immersion in the task. Although linear mapping is widely used, it falls short in providing a truly realistic experience to the operator due to variations in human sensitivity to different forces.

Inspired by [18], we formulate the force feedback model as an exponential function as follows, making it more sensitive to small forces and less sensitive to large forces.

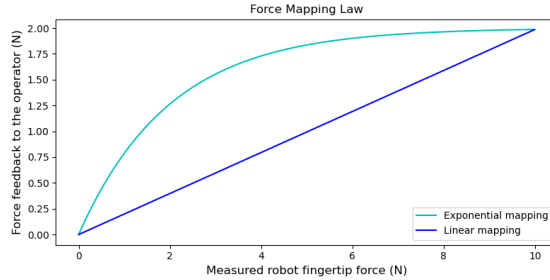


**Fig. 4.** Diagram of the force mapping law.

$$F^H = \sigma(-e^{\tau F^R} + \xi) \quad (9)$$

Where  $F^H$  denotes the force fed back to the human and  $F^R$  denotes the force perceived by the robot,  $\sigma = 2$ ,  $\tau = -0.5$ ,  $\xi = 1$ . Notably, we have limited the range of force feedback to ensure comfortable operation.

## 5 Experiment

### 5.1 Experimental Setup

The overall experimental setup consisted of :

- The data glove is equipped with 19 optical fibers, 15 of which are attached to the DIP, PIP, and MCP joints of the index, middle, ring, and little finger, as well as the IP, MCP, and CMC joint of the thumb, with which the flexion/extension angles are measured. Additionally, 4 fibers are attached between each of the five fingers, with which the abduction/adduction angles are measured.
- A hand exoskeleton is positioned on the dorsum of the hand and is capable of providing a maximum force feedback of 6.5N at each of the five fingertips.
- Three IMUs are affixed to the upper arm, forearm, and hand. These IMUs provide orientation information relative to the global coordinate system. The orientation is represented by quaternions and is based on the three-dimensional angular velocity, acceleration, and magnetic field.
- A CASIA Hand, with 21 degrees of actuation and 25 human-like degrees of freedom, including 16 on the fingers, 5 on the thumb, 2 on the palm, and 2 on the wrist. At each fingertip, a Contactile Force Sensor is attached to provide 3D force information from the slave side.
- A KUKA LBR iiwa with 7 degrees of freedom.

### 5.2 Simulation Experiments

To empirically validate the effectiveness of the hand motion mapping method, we present several mappings from MANO to CASIA Hand in Fig.5. The experimental results demonstrate that the method adequately considers factors such as fingertip position, joint angle, and self-collision, resulting in visually plausible outcomes.

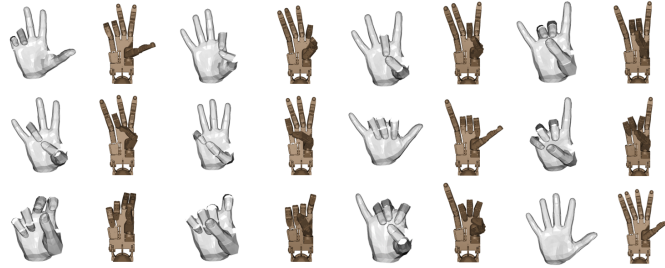


**Fig. 5.** Hand motion mapping results between the MANO and the CASIA Hand.

For further validation, we conducted a comparative evaluation with direct Cartesian mapping and direct joint mapping in the MuJoCo[19]. This evaluation is illustrated in Fig.6, where we selected two objects for precision grasp and power grasp scenarios. The results demonstrate that our method outperforms both direct Cartesian mapping and direct joint mapping approaches, achieving successful outcomes in both precision grasp and power grasp tasks.

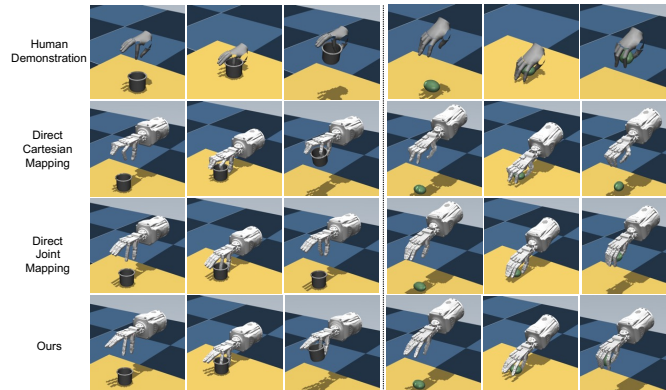


**Fig. 6.** Methods compared on the precision grasp task (left) and power grasp task (right).

### 5.3 Real-world Experiments

To further verify the system’s reliability, we conducted three physical experiments in the real world. Two operators participated and were instructed to wear the data glove, hand exoskeleton, and IMUs correctly. They then completed the necessary calibration steps and warm-up exercises before engaging in teleoperation tests.

1)Grasping tasks for 3D printed rigid objects: In this experiment, the robot grasps the object standing upright on the table, lifts it to at least 5 cm above the table, and holds it for at least 5 seconds, as shown in Fig.7.

2)Stacking blocks task: In this experiment, the robot first picks up the red block and places it in the given position, then returns to the initial pose, picks up the green block and stacks it on top of the red block, and finally repeats the above process to stack the yellow block on top of the green block. This teleoperation process is illustrated in Fig.8.



**Fig. 7.** Grasping tasks for 3D printed rigid objects. Top row, left to right: bottle, glasses, hammer, teapot, cell phone. Bottom row, left to right: wine glass, binoculars, cleanser bottle, headphones, flashlight.

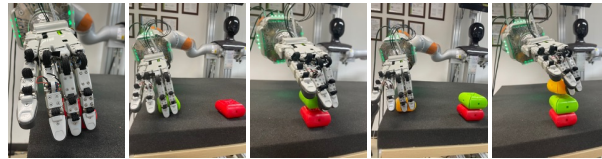


**Fig. 8.** Stacking blocks task. The teleoperation process is shown from left to right.

3) Grasping tasks for non-rigid objects: In this experiment, the robot delicately grasps the flexible and deformable object from the table, lifting it to a minimum height of 5 cm above the surface. Throughout the process, the robot ensures that the object remains relatively free from significant deformation, as demonstrated in Fig.9.

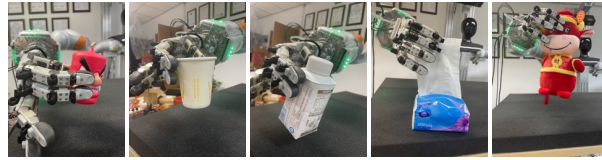


**Fig. 9.** Grasping tasks for non-rigid objects. Left to right: toy candle, dixie cup, yogurt box, tissue, doll.

Fig. 10 displays the average success rates for each task, with each operator performing the tasks five times within a three-minute time limit. Grasping rigid 3D printed objects requires precise control of the robot hand to achieve a reasonable grasp posture, posing significant challenges. Failures in this task often occur due to object pose changes resulting from collisions between the object and the fingers. Notably, this phenomenon is more pronounced when grasping objects such as glasses, hammers, and teapots. The stacking blocks task demands accurate control of the robot arm to precisely stack blocks on top of each other, given the small surface area of the blocks. Challenges in this task include inaccurate stacking positions, arm shaking, and premature or delayed release of objects, resulting in block slippage and task failure. When grasping non-rigid objects, operators adjust their hand poses based on force feedback from the hand exoskeleton to minimize object deformation during the process. However, we observed that the effectiveness of the hand exoskeleton varied de-

pending on the operator. When operators exhibited excessive resistance or were unprepared for the force feedback, the hand exoskeleton proved ineffective or even counterproductive.

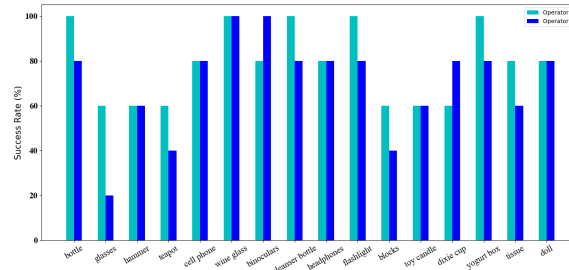


Fig. 10. Success rate of teleoperation tasks.

## 6 Conclusion

This paper presents a framework for human-like dexterous manipulation via teleoperation for the anthropomorphic hand-arm robotic system. Our framework incorporates a wearable system comprising a data glove, three IMUs, and a hand exoskeleton to capture human hand-arm motion and provide force feedback. Additionally, we have developed an anthropomorphic robotic system consisting of a robotic arm and a CASIA Hand equipped with force sensors at the fingertips for executing operations. To enable seamless interaction, we have designed a set of mapping algorithms for translating human motion to robot motion and robot forces to human forces. Experiments conducted on the simulation platform and real-world platform demonstrated the effectiveness and reliability of the system.

Future work involves incorporating virtual reality technology to provide visual feedback, enhancing the teleoperation experience for smoother control. Additionally, there are plans to extend the teleoperation capabilities from a single hand-arm robot to a dual hand-arm robot and delve into the realm of human-robot fusion technology.

**Acknowledgement** This work was supported in part by the National Natural Science Foundation of China under Grants (91748131, 62006229, and 61771471), in part by the Strategic Priority Research Program of Chinese Academy of Science under Grant XDB32050106, and in part by the InnoHK Project.

## References

1. Duan, H., Wang, P., Li, Y., Li, D., Wei, W.: Learning human-to-robot dexterous handovers for anthropomorphic hand. *IEEE Transactions on Cognitive and Developmental Systems* pp. 1–1 (2022). <https://doi.org/10.1109/TCDS.2022.3203025>
2. Li, Y., Wei, W., Li, D., Wang, P., Li, W., Zhong, J.: Hgc-net: Deep anthropomorphic hand grasping in clutter. In: 2022 International Conference on Robotics and Automation (ICRA). pp. 714–720 (2022). <https://doi.org/10.1109/ICRA46639.2022.9811756>

3. Wei, W., Li, D., Wang, P., Li, Y., Li, W., Luo, Y., Zhong, J.: Dvvgg: Deep variational grasp generation for dextrous manipulation. *IEEE Robotics and Automation Letters* **7**(2), 1659–1666 (2022). <https://doi.org/10.1109/LRA.2022.3140424>
4. Wei, W., Wang, P., Wang, S.A.: Generalized anthropomorphic functional grasping with minimal demonstrations. *ArXiv abs/2303.17808* (2023)
5. Li, W., Wei, W., Wang, P.: Continual learning for anthropomorphic hand grasping. *IEEE Transactions on Cognitive and Developmental Systems* (2023)
6. Li, W., Wei, W., Wang, P.: Neuro-inspired continual anthropomorphic grasping. *Iscience* (2023)
7. Li, R., Wang, H., Liu, Z.: Survey on mapping human hand motion to robotic hands for teleoperation. *IEEE Transactions on Circuits and Systems for Video Technology* **32**(5), 2647–2665 (2021)
8. Qin, Y., Su, H., Wang, X.: From one hand to multiple hands: Imitation learning for dexterous manipulation from single-camera teleoperation. *IEEE Robotics and Automation Letters* **7**(4), 10873–10881 (2022)
9. Zahlner, S., Hirschmanner, M., Patten, T., Vincze, M.: Teleoperation system for teaching dexterous manipulation. *Google Scholar* (2020)
10. Li, S., Ma, X., Liang, H., Görner, M., Ruppel, P., Fang, B., Sun, F., Zhang, J.: Vision-based teleoperation of shadow dexterous hand using end-to-end deep neural network. In: 2019 International Conference on Robotics and Automation (ICRA). pp. 416–422. *IEEE* (2019)
11. Liu, G., Geng, X., Liu, L., Wang, Y.: Haptic based teleoperation with master-slave motion mapping and haptic rendering for space exploration. *Chinese Journal of Aeronautics* **32**(3), 723–736 (2019). <https://doi.org/https://doi.org/10.1016/j.cja.2018.07.009>
12. Chattaraj, R., Bepari, B., Bhaumik, S.: Grasp mapping for dexterous robot hand: A hybrid approach. In: 2014 Seventh International Conference on Contemporary Computing (IC3). pp. 242–247. *IEEE* (2014)
13. Meattini, R., Chiaravalli, D., Biagiotti, L., Palli, G., Melchiorri, C.: Combined joint-cartesian mapping for simultaneous shape and precision teleoperation of anthropomorphic robotic hands. *IFAC-PapersOnLine* **53**(2), 10052–10057 (2020)
14. Liang, Y., Li, W., Wang, Y., Xiong, R., Mao, Y., Zhang, J.: Dynamic movement primitive based motion retargeting for dual-arm sign language motions. In: 2021 IEEE International Conference on Robotics and Automation (ICRA). pp. 8195–8201. *IEEE* (2021)
15. Romero, J., Tzionas, D., Black, M.J.: Embodied hands: Modeling and capturing hands and bodies together. *arXiv preprint arXiv:2201.02610* (2022)
16. Handa, A., Van Wyk, K., Yang, W., Liang, J., Chao, Y.W., Wan, Q., Birchfield, S., Ratliff, N., Fox, D.: Dexpilot: Vision-based teleoperation of dexterous robotic hand-arm system. In: 2020 IEEE International Conference on Robotics and Automation (ICRA). pp. 9164–9170. *IEEE* (2020)
17. Johnson, S.G.: The nlopt nonlinear-optimization package. <http://github.com/stevengj/nlopt>
18. Park, S., Park, Y., Bae, J.: Performance evaluation of a tactile and kinesthetic finger feedback system for teleoperation. *Mechatronics* **87**, 102898 (2022)
19. Todorov, E., Erez, T., Tassa, Y.: Mujoco: A physics engine for model-based control. In: 2012 IEEE/RSJ international conference on intelligent robots and systems. pp. 5026–5033. *IEEE* (2012)